Food Chemistry: X 24 (2024) 102030

Contents lists available at ScienceDirect

Food Chemistry: X

journal homepage: www.sciencedirect.com/journal/food-chemistry-x

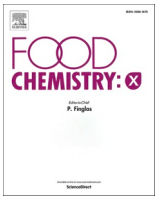

Ultrasensitive colorimetric immunoassay for aflatoxin B_1 detection in lotus seed powder based on enhanced catalysis of Au@Pt with in situ deposition of PtNPs

Lei Zhang [a,1], Huiqiang Huang [a,1], Mengyao Liao [a,1], Chenghua Luo [a], Qiuyue Wu [a], Rentang Huang [a], Hongmei Liu [c], Xiangsheng Zhao [b,*], Shumei Wang [a,*]

[a] Key Laboratory of Digital Quality Evaluation of Traditional Chinese Medicine, National Administration of Traditional Chinese Medicine & Guangdong Provincial Traditional Chinese Medicine Quality Engineering and Technology Research Center, Guangdong Pharmaceutical University, Guangzhou 510006, China
[b] Hainan Provincial Key Laboratory of Resources Conservation and Development of Southern Medicine & Hainan Branch of the Institute of Medicinal Plant Development, Chinese Academy of Medical Sciences and Peking Union Medical College, Haikou 570311, China
[c] cademy of National Food and Strategic Reserves Administration, No.11 Baiwanzhuang Str, Xicheng District, Beijing 100037, China

ARTICLE INFO

Keywords:
Aflatoxin
Nanozyme
In situ deposition
Immunoassay
Rapid detection

ABSTRACT

The enzyme-linked immunosorbent assay (ELISA) is a powerful and high-throughput method for detecting aflatoxin B_1 (AFB_1) in food. However, the susceptibility of native enzymes to environmental factors limits their potential applications. This study introduces the combined use of precious metal nanozymes as alternative catalysts to improve the performance of traditional ELISA. Au@Pt can be linked to antibodies to construct recognition probes, onto which platinum nanoparticles (PtNPs) are ingeniously deposited in situ to amplify the detection signal, thereby increasing the sensitivity. The proposed PtNP-enhanced Au@Pt-ELISA exhibited excellent resistance against matrix interference for AFB_1 detection in lotus seed powder and achieved a detection limit of 1.6 pg/mL (0.32 μg/kg), which was approximately six times lower than that of traditional ELISA. Furthermore, the results of the proposed approach were strongly correlated with LC–MS/MS analysis results for real samples ($r = 0.9888$, $n = 13$). This study offers a new strategy for AFB_1 monitoring in a complex matrix.

1. Introduction

Nelumbo nucifera Gaertn., which is commonly referred to as lotus, is an ancient plant from the *Nelumbonaceae* family. This plant has been used as a food in Asia for over 7000 years (Arooj et al., 2021). The cultivation of the lotus revolves primarily around the use of its rhizomes, flowers, leaves, and seeds. Lotus seeds, in particular, are renowned for their nutritional value, containing 61–62 % carbohydrates, 16–21 % protein, 2.40–3 % crude fat, and 5–9 % moisture content (Dunno et al., 2022). Moreover, in addition to these vital nutrients, lotus seeds are rich in bioactive compounds such as flavonoids, glycosides, phenolic compounds, and alkaloids (Arooj et al., 2021), contributing to their pharmacological properties that are beneficial for human health. These properties mainly include antioxidant (Yu et al., 2021), antiobesity (Cao et al., 2018), and lipid-lowering effects (Zeng et al., 2023).

The high levels of proteins and polysaccharides present in lotus seeds render them susceptible to contamination by toxigenic fungi, particularly *Aspergillus* spp., which is a frequent contaminant (Elamin et al., 2024). Aflatoxins (AFs), which are produced principally by *Aspergillus flavus* and *Aspergillus parasiticus*, are a group of harmful secondary metabolites, with over 20 varieties of AFs and their derivatives identified thus far (Magdalena Pisoschi et al., 2023). Notably, aflatoxin B_1 (AFB_1) is the most toxic type and was classified as a group I carcinogen by the International Agency for Research on Cancer (IARC) in 1993. Further, when ingested by mammals through AFB_1-contaminated feed, AFB_1 is metabolized into aflatoxin M_1 (a group 1 carcinogen according to the 2002 IARC report), which is later excreted into milk. This process can lead to the secondary contamination of milk consumers (Xiong et al., 2022).

Reports have revealed the incidence of aflatoxin contamination in lotus seeds. In accordance with our previous findings, the occurrence rate of AFB_1 in lotus seeds was reported to be 32 % (Qin et al., 2020).

* Corresponding authors.
E-mail addresses: xszhao@implad.ac.cn (X. Zhao), smwang@gdpu.edu.cn (S. Wang).
[1] These authors contributed equally to this work

https://doi.org/10.1016/j.fochx.2024.102030
Received 26 June 2024; Received in revised form 8 November 2024; Accepted 20 November 2024
Available online 23 November 2024

Moreover, lotus seeds can become contaminated with *A. flavus* and AFs before harvest (Elamin et al., 2024). Given the vulnerability of lotus seeds to aflatoxin contamination, devising an effective detection method has become a research priority. However, AFB_1 detection methods have been designed primarily to detect AFB_1 in raw lotus seed materials. There is still a research gap concerning the detection of AFB_1 in processed lotus seed products that needs to be addressed.

In the early stages, high-performance liquid chromatography (HPLC) and liquid chromatography–tandem mass spectrometry (LC–MS/MS) were employed as analytical techniques for assessing aflatoxin levels in lotus seeds (Liu et al., 2013). Several rapid detection methods have subsequently emerged in recent years to supplement these instrumental analysis approaches. These methods include the enzyme-linked immunosorbent assay (ELISA) (Chu et al., 2015), immunochromatographic test strips utilizing gold nanoparticles (AuNPs) or fluorescent nanoparticles (Jia et al., 2021), and electrochemical immunosensors (Deng et al., 2024). Among these methods, ELISA is well-suited for efficient high-throughput screening. However, one notable downside of ELISA is that native enzymes such as horseradish peroxidase (HRP), which is commonly used in the process, are susceptible to environmental factors such as variations in pH and temperature (Saud Al-Bagmi et al., 2019). This susceptibility could lead to hindrances such as the potential inhibition of catalytic activity.

Nanozymes, which are composed of either inorganic or organic nanomaterials with distinct nanostructures (Zhang & Liu, 2020), offer several advantages over native enzymes. These include cost-effectiveness, sturdiness under harsh conditions, and ease of production. Their unique physicochemical properties are derived from their elemental compositions which can include precious metal materials, carbon-based materials, or metal oxides, among other materials (Villalba-Rodríguez et al., 2023). Among these types of nanozymes, precious metal nanozymes have garnered considerable interest in diverse research and practical domains owing to their facile fabrication and biofunctionalization attributes. For example, positively charged AuNPs have been utilized as peroxidase mimics to enable the colorimetric detection of hydrogen peroxide and glucose (Jv et al., 2010). In an innovative approach, Deng and colleagues utilized target-induced shielding to inhibit the peroxidase-like catalytic activity of AuNPs for colorimetric detection and sensing of sulfide (Deng et al., 2014). Their research indicates that unlabeled AuNPs exhibit favorable enzyme mimetic properties. However, when biomolecules such as DNA or antibodies are absorbed onto AuNPs to create an immunogold probe, they can hinder the substrate binding necessary for the peroxidase-like reaction (Lou et al., 2018; Park et al., 2011). Consequently, there has been a consistent effort to develop and apply nanozymes with enhanced activity.

Compared with their monometallic counterparts, bimetallic nanozymes exhibit superior mimetic enzyme activity, which is due primarily to the interactions between metal ions. In recent studies, emphasis has been placed on bimetallic Au@Pt core–shell nanostructures owing to their synergistic properties and easy surface functionalization (Hendrickson et al., 2023; Wei et al., 2020; Zhang et al., 2018; Zhang et al., 2022). In this work, we synthesized popcorn-like Au@Pt core–shell structures (Zheng et al., 2014) to serve as a peroxidase mimics for developing peroxidase-labeled antibody probes. However, a decrease in mimetic activity similar to that of AuNP nanozymes was observed after the conjugation of antibodies. This alteration results in an increased dosage of antibodies being required, consequently reducing the detection sensitivity and increasing the testing costs. Considering the excellent peroxidase-like activity of platinum nanomaterials (PtNPs) (Gao et al., 2013; Li et al., 2015), we focused on enhancing the catalytic activity of immunoprobes by incorporating PtNPs into antibody-conjugated Au@Pt. We propose a design that utilizes Au@Pt nanozymes as carriers to construct nano enzymatic probes and to amplify detection signals via in suit deposition of PtNPs (Scheme 1). This innovative strategy aims to establish a straightforward, fast, and highly sensitive direct competition immunoassay for the high-throughput screening of AFB_1 in lotus seed powder, which is a commonly consumed processed product of lotus seeds, with limited attention given to AFB_1 contamination.

2. Materials and methods

2.1. Materials

Anti-AFB_1 monoclonal antibody and AFB_1-bovine serum albumin (BSA) antigen were purchased from Shenzhen Anti Biological Technology Co., Ltd. Horseradish peroxidase-labeled goat anti-mouse secondary antibody (IgG-HRP) was purchased from Nanning Blue Light Biotechnology Co., Ltd. Standard solutions of AFB_1, AFB_2, AFG_1, and AFG_2 were

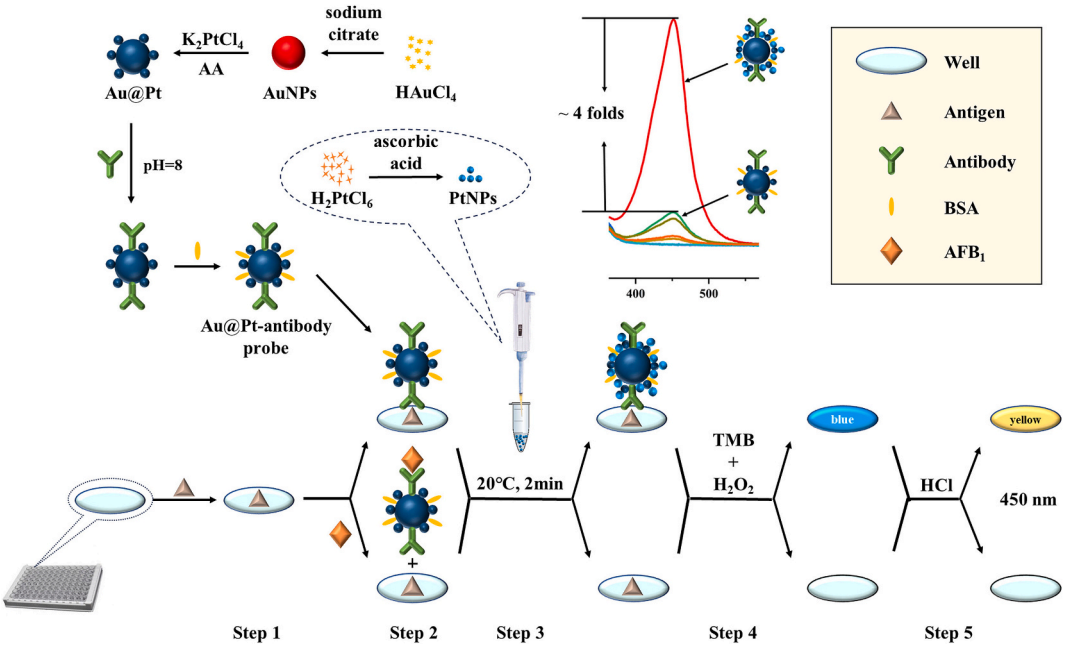

Scheme 1. Schematic illustration of PtNP-enhanced Au@Pt-ELISA for AFB_1.

purchased from Pribolab (Singapore). The isotope internal standard [$^{13}C_{17}$]-AFB_1 was purchased from Romer Labs (Tulln, Austria). Potassium chloroplatinate, chloroauric acid ($HAuCl_4{\cdot}3H_2O$), chloroplatinic acid ($H_2PtCl_6{\cdot}6H_2O$), BSA, and 3,3′,5,5′-tetramethylbenzidine (TMB) were purchased from Aladdin (China). Gelatin was purchased from Nanjing Dulai Biotechnology Co., Ltd. Hydrogen peroxide (30 % H_2O_2) was purchased from Shanghai Wokai Biotechnology Co., Ltd. Citric acid ($C_6H_8O_7$), ascorbic acid ($C_6H_8O_6$) and Tween 20 were purchased from Xilong Scientific Co., Ltd.

The buffers employed in this work consisted of 50 mM carbonate/bicarbonate buffer at pH 9.6 as the coating buffer, 10 mM phosphate-buffered saline (PBS) containing 137 mM NaCl, 2.7 mM KCl, 10 mM Na_2HPO_4, and 1.8 mM KH_2PO_4, and washing buffer (PBST) composed of a solution containing 0.1 % Tween 20 in PBS buffer with a pH of 7.4.

2.2. Synthesis of AuNPs

AuNPs were prepared following our previously reported method (Huang et al., 2023). A sodium citrate solution (2.2 mM, 150 mL) was heated to 70 °C, and then a potassium carbonate solution (150 mM, 1 mL) and tannic acid solution (2.5 mM, 0.1 mL) were added under constant stirring. Subsequently, rapid injection of $HAuCl_4$ (25 mM, 1 mL) initiated a 5-min reaction to form AuNP seeds (L0). A portion of the obtained AuNP seed (L0) solution (55 mL) was removed and replenished with sodium citrate (2.2 mM, 55 mL) before being heated to 70 °C. The addition of $HAuCl_4$ (25 mM, 0.5 mL) led to a 10-min reaction, and additional $HAuCl_4$ (25 mM, 0.5 mL) was injected to continue the 10-min reaction, resulting in the production of AuNPs (L1). This growing step including sample dilution and two injections of $HAuCl_4$ was repeated until the L4 generation.

2.3. Synthesis of Au@Pt Nanozymes

Au@Pt nanozymes with a core/shell structure were synthesized following the protocol described by Zhang et al. (2022), with slight modifications. In a three-necked flask, 2 mL of AuNPs (L4) were introduced and heated to 80 °C. Subsequently, 2 mL of potassium tetrachloroplatinate (1 mM) was swiftly added, followed by the gradual addition of 1 mL of ascorbic acid (10 mM). The reaction proceeded for 30 min to yield the Au@Pt solution, which was then stored at 4 °C for future use.

2.4. Immobilization of the anti-AFB_1 monoclonal antibody on Au@Pt

The previously prepared Au@Pt solution (250 μL) was transferred into an Eppendorf tube, and the pH was adjusted to 8.0 with a potassium carbonate solution. Subsequently, 15 μL of AFB_1 antibody (0.1 mg/mL) was added to the mixture, which was gently oscillated for 15 min. Subsequently, equal volume (25 μL) of 10 % BSA and 1 % polyethylene glycol (PEG) solution were added sequentially, with an additional 15 min of oscillation. The mixture underwent centrifugation at 4 °C and 12,000 rpm for 20 min, after which the supernatant was removed. The residue was dissolved again in a solution consisting of equal parts of 1 % BSA and 0.1 % PEG.

2.5. Synthesis of PtNPs

PtNPs were prepared as described in the literature (Li et al., 2018). In a typical synthesis, 10 μL of H_2PtCl_6 solution (100 mM) was combined with 900 μL of distilled water and heated at 80 °C for 20 min. Subsequently, 100 μL of a 400 mM ascorbic acid solution was swiftly added and thoroughly mixed, and the mixture was then incubated at 80 °C for 30 min. The obtained PtNPs were then centrifuged at 4 °C and 12,000 rpm for 20 min. The supernatant was discarded, and the precipitate was resuspended in distilled water.

2.6. Au@Pt based Nanozyme immunoassay enhanced by PtNPs

The AFB_1-BSA antigen was diluted with a coating buffer and added to a 96-well plate (100 μL per well). The plate was incubated overnight at 4 °C, followed by three washes with PBST. Then, various concentrations of AFB_1 standard or sample solution were added. An equal amount of Au@Pt-anti-AFB_1 antibody conjugate (abbreviated as the Au@Pt probe), which had been diluted 15 times with 0.1 % gelatin, was added to each well, and the mixture was incubated at 37 °C for 1 h before being washed four times with PBST. A dilution of the PtNPs was then prepared and added to each plate well (100 μL per well), followed by an enhancement step at 20 °C for 2 min and five subsequent washes with distilled water. Each well was subsequently treated with a mixed TMB-H_2O_2 solution (100 μL) and allowed to react for 15 min. The reaction was terminated by the addition of 50 μL of 1 M hydrochloric acid per well, and the optical density (OD) value of the reaction product was measured at 450 nm with a Spark microplate photometer (Tecan, Switzerland).

2.7. Traditional indirect competition enzyme immunoassay

The plate underwent a series of steps, including coating, washing, blocking, and a second washing cycle, as detailed in Section 2.6. The AFB_1 standard solution (50.0 μL) and an equal volume of an anti-AFB_1 monoclonal antibody solution (50.0 μL) were introduced into the wells, and the plate was incubated at 37 °C for 1 h. After incubation, the plate was washed three times with PBST, after which IgG-HRP solution was added to the wells, followed by another incubation period of 1 h and four subsequent washes with PBST. A mixed TMB-H_2O_2 solution (100 μL/well) was then dispensed into the wells for a color reaction. After 15 min, the reaction was stopped by the addition of 50.0 μL of 1 M hydrochloric acid to each well. The OD value of the resulting yellow product was determined at 450 nm.

2.8. Kinetic analysis

The catalytic activities of unmodified Au@Pt, the Au@Pt probe, the PtNP-enhanced Au@Pt probe, and HRP were assessed through the determination of the apparent steady-state kinetic parameters for the TMB-H_2O_2 chromogenic reaction. Experimental data were gathered by altering the concentration of TMB at a constant H_2O_2 concentration and vice versa. The reactions were conducted at 30 °C using 0.49 nM unmodified Au@Pt or 50.0 nM HRP for comparison in a 0.05 M Na_2HPO_4-citric acid buffer at pH 5.0. Furthermore, for the Au@Pt probe and PtNP-enhanced Au@Pt probe, the mimetic activity was analyzed in situ following an immunological reaction in the microplate. Typical Michaelis–Menten curves were generated for unmodified Au@Pt, the Au@Pt probe, the PtNP-enhanced Au@Pt probe, and HRP using TMB and H_2O_2 as substrates over a specified range of concentrations. The Michaelis–Menten constant (K_m), which is indicative of the enzyme–substrate affinity, was determined through a Lineweaver–Burk plot (Feng et al., 2017):

$$\frac{1}{\nu} = \left(\frac{K_m}{V_{max}}\right)\left(\frac{1}{[S]}\right) + \left(\frac{1}{V_{max}}\right)$$

where ν is the initial velocity, V_{max} is the maximal reaction velocity, and $[S]$ is the substrate concentration.

2.9. Real application of the PtNP-enhanced Au@Pt-based immunoassay for AFB_1 detection

Eighteen batches of lotus seed powder samples were randomly purchased from the Chinese market, and the sample information is presented in Table S1. Each sample (1.0 g) was transferred into a 10 mL centrifuge tube, after which 5 mL of an acetonitrile–water mixture

(90:10, *v/v*) was added. The contents were vigorously vortexed for 3 min, followed by centrifugation at room temperature for 5 min at a speed of 10,000 rpm. The resulting supernatant was transferred and diluted 40-fold with a PBS solution containing 0.01 % Tween 20 to prepare the test solution for immunoassay. The positive samples were subsequently confirmed through stable isotope dilution and LC–MS/MS analysis, with the experimental parameters detailed in the Supplementary Materials.

3. Results and discussion

3.1. Sensing mechanism of the colorimetric immunoassay

The experimental procedure illustrated in Scheme 1 involved the initial coating of microtiter wells with BSA-AFB_1 as the antigen. A sample or AFB_1 standard solution combined with the Au@Pt probe was subsequently added to the coated wells. This facilitated a competitive binding process between the coated antigen and AFB_1 to the antibodies. Before colorimetric assessment, PtNPs were introduced and allowed to selectively deposit onto Au@Pt at a specific pH, thereby amplifying the peroxidase-like activity of the Au@Pt probe. Consequently, the concentration of AFB_1 could be determined by evaluating the catalytic performance of PtNP-enhanced Au@Pt in catalyzing TMB oxidation with H_2O_2 as an electron acceptor.

3.2. Characteristics of the Au@Pt nanoparticles

Various synthesis methods have been developed for the preparation of Au@Pt (Feng et al., 2017; He et al., 2011; Wei et al., 2020). In this study, we selected a relatively straightforward and time-efficient synthesis method to ensure the reproducibility of the synthesis process. The obtained Au@Pt nanoparticles were characterized via UV − vis absorption spectroscopy and transmission electron microscopy (TEM). As shown in Fig. 1(A), AuNPs with an average diameter of 11.5 nm exhibited an orange–red color, and a prominent UV–visible absorption peak was observed at 516.5 nm. Upon introduction of a platinum (Pt) shell, the solution turned black, with the disappearance of the UV–visible absorption peak at 516.5 nm. The TEM images in Fig. 1(B) revealed a morphological transformation of the nanoparticles from spherical to "popcorn" shaped, indicating the successful deposition of the Pt shells. These findings align with those from a previous study (Wang et al., 2018).

3.3. Optimization of the preparation of the Au@Pt-antibody conjugates

3.3.1. pH of the coupling solution

Biomolecules can adhere to the surface of Au@Pt through electrostatic adsorption, forming a dense electronic layer on the substrate (Zeng et al., 2019). Adjusting the pH can impact the electronic properties of the Au@Pt surface, which in turn affects the binding efficiency of biomolecules. In this study, the pH of the coupling solution was adjusted to 6, 7, 8, 9, or 10 using 150 mM K_2CO_3 before the antibody was introduced for coupling. The optimal pH was determined on the basis of the B_0 value (the OD value in the absence of AFB_1) and the inhibition rate (B/B_0, which represents the ratio of the OD values with and without 0.0625 ng/mL AFB_1). The results revealed a decrease and then an increase in the inhibition rate between pH values of 6 and 9, reaching a minimum at pH 7, as shown in Fig. S1(A). Conversely, the B_0 value increased but then decreased from pH 6 to 10, peaking at pH 8. While the inhibition rate was modestly greater at pH 8 than at pH 7, the B_0 value increased significantly. Considering both factors, a pH of 8 was determined to be the optimal condition in this study.

3.3.2. Amount of antibody used for conjugate construction

The anti-AFB_1 monoclonal antibody binds specifically to the antigen, and the amount of antibody attached to the Au@Pt surface significantly impacts the OD value and sensitivity of the assay. To determine the optimal amount of antibody, varying volumes of AFB_1 monoclonal antibody (0.1 mg/mL), specifically 2.5, 5, 7.5, 10, 12.5, 15, and 17.5 μL, were individually added to the Au@Pt solution for coupling. The evaluation was based on criteria that included the measured B_0 value and inhibition rate, similar to pH optimization. According to Fig. S1(B), the B_0 value initially increased but then decreased, reaching a peak at 15 μL within the range of 2.5–17.5 μL. Simultaneously, the B/B_0 value decreased, followed by an increase, with its minimum at 15 μL. Consequently, the optimal antibody amount was determined to be 15 μL (0.1 mg/mL).

3.4. Optimization of enhancement conditions for PtNPs

On the basis of prior studies (Lee et al., 2010; Taron et al., 2020), AuNPs clearly exhibit considerable inhibition of their enzyme-like activity upon adsorption by biomolecules. Our research revealed a similar issue with Au@Pt. Typical Michaelis–Menten curves were generated within a specific range of H_2O_2 or TMB concentrations, as illustrated in Fig. S2. K_m was calculated via the Lineweaver–Burk equation. The results (Table 1) indicated a lower K_m value of Au@Pt than that of HRP toward TMB, whereas conversely, the K_m value of Au@Pt was higher than that of HRP toward H_2O_2. This observation is in line with previous research (Mora-Sanz et al., 2020). Furthermore, upon antibody modification, the K_m values of Au@Pt toward both TMB and H_2O_2 increased, indicating a reduced affinity of antibody-labeled Au@Pt for TMB and H_2O_2 (Wei et al., 2020).

Recently, an in situ enhancement method has been employed to

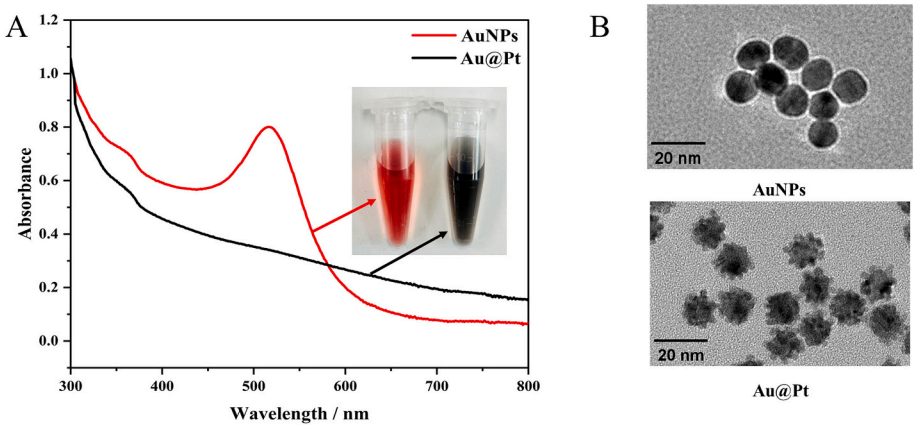

Fig. 1. (A) UV–vis spectrums and (B) TEM images of AuNPs and Au@Pt.

Table 1
K_m and V_{max} value of HRP, Au@Pt, Au@Pt probe, PtNP-enhanced Au@Pt probe to TMB and H_2O_2.

	Concentration (nM)	TMB		H_2O_2	
		K_m (mM)	V_{max} (10^{-7} M·s^{-1})	K_m (mM)	V_{max} (10^{-8} M·s^{-1})
HRP	50.0	0.942	9.28	0.215	10.7
Au@Pt	0.49	0.600	6.81	18.7	6.13
Au@Pt probe		0.774	4.33	30.7	8.84
PtNP-enhanced Au@Pt probe		0.879	5.41	13.3	7.31

amplify the detection signal of AuNP-based ELISA. To illustrate, a gold or platinum shell has been formed onto the antibody-coated AuNP probes by reducing gold or platinum-enhancing solution, thereby initiating the catalytic activity of these probes (Li et al., 2018; Taron et al., 2020). These methods exhibit a common feature in that the enhancement process occurs after the specific recognition between the antibody probe and target molecule, thus circumventing the need for catalysts to be modified with detection antibodies and preventing the diminished catalytic activity resulting from the obstruction of catalytic active sites. PtNPs are recognized for their exceptional catalytic properties, which catalyze the decomposition of H_2O_2 to generate O_2 (Zhu et al., 2015). Therefore, we prepared PtNPs and modified them onto the Au@Pt probe via an in situ deposition method. This resulted in the generation of synergistic composites that merged the superior characteristics of both materials (Li et al., 2024), which harnessed the benefits of the easy surface modification of Au@Pt alongside the considerable catalytic effectiveness of PtNPs.

3.4.1. *pH of PtNP enhancing solution*

We hypothesized two potential mechanisms for the deposition of PtNPs onto the Au@Pt probe: electrostatic interactions leading to adsorption onto the antibody or BSA protein surface and self-assembly onto the Au@Pt surface to form nanoclusters. Both of these mechanisms are related to the pH of the reaction system (Yuan et al., 2022). Hence, we performed a comparative analysis of various pH values ranging from 5 to 10. As shown in Fig. 2(A), pH 6 was optimal on the basis of assessments of B_0 values and inhibition rates. Additionally, the findings depicted in Fig. 2(B) supported the signal amplification attribute of the PtNPs. This observation indicates that the development of a yellow color occurs within the system incorporating the Au@Pt probe alongside H_2O_2 and TMB. Furthermore, following treatment with the PtNP enhancing solution, the yellow color markedly increased in intensity.

Notably, a comparison between the immunoassays with and without the Au@Pt probe (Fig. S3) revealed substantial nonspecific adsorption at relatively lower pH values, such as pH 5, and higher pH values, such as pH 10. However, lower nonspecific adsorption was observed at pH 6 and pH 7. This observation suggests that by regulating the pH, we can selectively deposit PtNPs on the Au@Pt probe. Nevertheless, we were unable to confirm whether the PtNPs were bound to the antibodies through electrostatic adsorption or to Au@Pt by self-assembly at this time.

3.4.2. *Enhancement time, concentration of PtNPs, and enhancement temperature*

To further improve the sensitivity of the proposed immunoassay, parameters such as the incubation time, PtNP solution concentration, and incubation temperature during the enhancement process were evaluated. As shown in Fig. 2(C-E), both the B_0 value and the inhibition rate were influenced by these factors. The optimal conditions were determined to be an enhancement time of 2 min, using a 500-fold dilution of PtNP solution, at an enhancement temperature of 20 °C. These conditions were found to provide a suitable sensitivity and detection range.

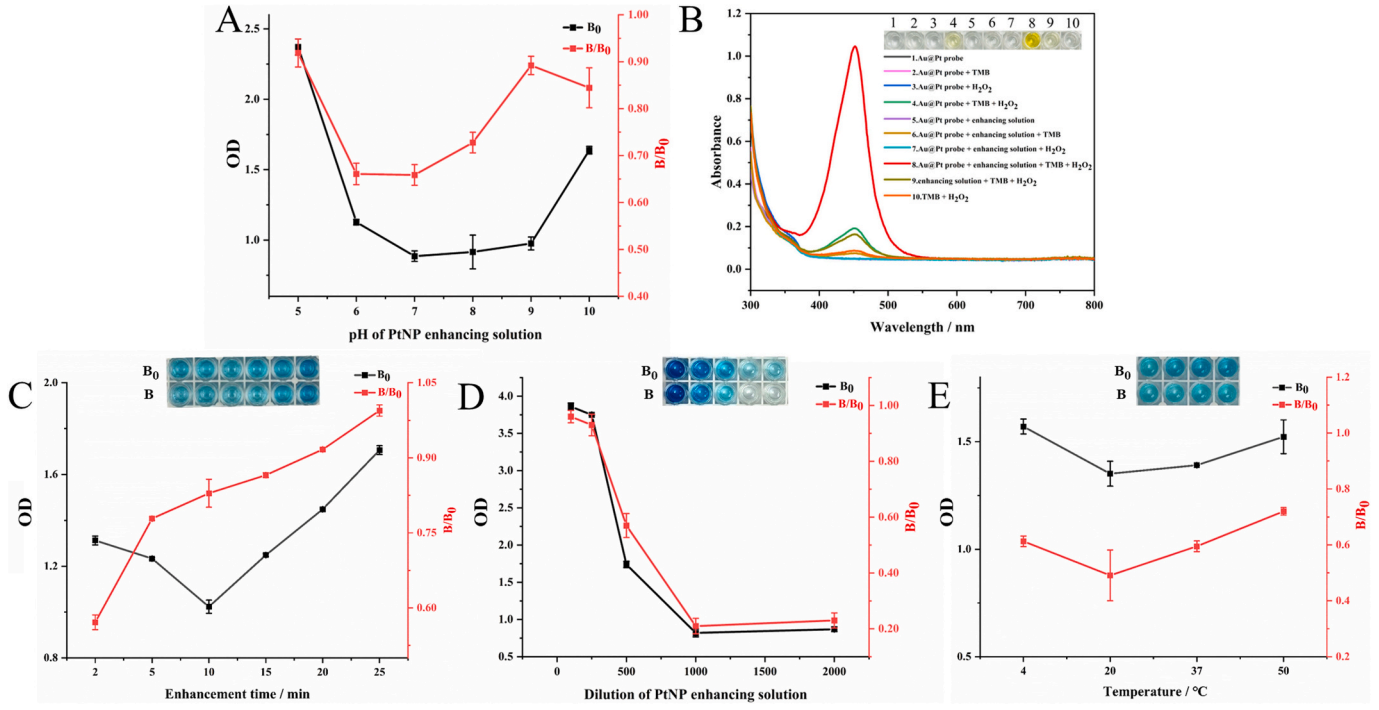

Fig. 2. (A) The different pH of PtNP enhancing solution; (B) UV–vis spectrums of the signal enhancing system containing 1. Au@Pt probe only, 2. Au@Pt probe + TMB, 3. Au@Pt probe + H_2O_2, 4. Au@Pt probe +TMB+ H_2O_2, 5. Au@Pt probe + PtNP enhancing solution, 6. Au@Pt probe + PtNP enhancing solution + TMB, 7. Au@Pt probe + PtNP enhancing solution + H_2O_2, 8. Au@Pt probe + PtNP enhancing solution + TMB+ H_2O_2, 9. PtNP enhancing solution + TMB+ H_2O_2, 10.TMB+ H_2O_2; The effects of (C) enhancement time, (D) dilution of PtNP enhancing solution, and (E) temperature.

3.5. Optimization of the TMB and H_2O_2 concentration in the chromogenic solution

The rate of the redox reaction catalyzed by the PtNP-enhanced Au@Pt probe is influenced by the concentrations of TMB and H_2O_2. Fig. S4(A) shows the effect of varying the TMB concentrations on the catalytic reaction. The B_0 value increased and eventually stabilized. Conversely, the inhibition rate initially decreased and then slightly increased, and it seemed to reach its minimal value at a concentration of 2.5 mM. With these factors in mind, a TMB concentration of 2.5 mM was selected for subsequent experiments. Additionally, the effect of the H_2O_2 concentration on the B_0 value and inhibition rate was further assessed within a range of 0.5 to 1.5 M. The results, illustrated in Fig. S4(B), demonstrated a consistent increase in the B_0 value. Moreover, the B/B_0 value first decreased and then increased, reaching a minimum at a concentration of 0.9 M. Consequently, a H_2O_2 concentration of 0.9 M was utilized for the experiment.

3.6. Characteristics of PtNP-enhanced Au@Pt Nanozymes

The HRTEM, HAADF-STEM, and EDS mapping images revealed no significant difference in shape between the Au@Pt probe and the PtNP-enhanced Au@Pt probe (Fig. 3). This could have been related to the lower deposition of PtNPs, as indicated by the ICP–OES results (Fig. S5). Compared with the pre-enhancement state, the proportion of Pt elements only increased by only approximately 1 %. Furthermore, we conducted TEM characterization of the PtNPs. Despite the suboptimal dispersion of PtNPs in the images (Fig. S6), it was still possible to observe that the size of each nanoparticle was similar to that of the surface platinum of Au@Pt. This result can also explain the lack of any noticeable difference in appearance in the TEM images before and after enhancement.

In Section 3.4.1, we concluded that by regulating the pH, PtNPs could be selectively deposited on the Au@Pt probe. However, the exact mechanisms underlying this process have not yet been clarified. The results shown in Fig. 3 enable us to hypothesize that PtNPs are more prone to self-assembly on Au@Pt, rather than binding themselves to antibodies or BSA proteins on the surface of Au@Pt. If protein binding indeed occurred, we would probably have seen gaps between the PtNPs (used for signal enhancement) and the surface platinum of Au@Pt in the TEM images, due to the inherent volume of the protein. However, no such gaps were observed.

A comparative analysis of the catalytic efficiency between of PtNP-enhanced Au@Pt probe, the Au@Pt probe, and unmodified Au@Pt was subsequently conducted. The results presented in Table 1 revealed that the K_m value for H_2O_2 of the PtNP-enhanced Au@Pt probe was 13.3 mM, which was 17.4 mM lower than that of the Au@Pt probe. Conversely, the K_m value for the TMB of the PtNP-enhanced Au@Pt probe was calculated to be 0.879 mM, which was slightly greater than that of the Au@Pt probe. K_m, which is a critical parameter, signifies the affinity between an enzyme and its substrate. Hence, we consider that the signal enhancement primarily stems from the increased affinity of H_2O_2 for the PtNP-enhanced Au@Pt probe. Furthermore, our observations indicate that the adsorption capability of H_2O_2 was notably higher in the PtNP-enhanced system than in the unmodified Au@Pt system. This highlights the effectiveness of PtNP enhancement as a strategy for signal amplification.

3.7. Optimization of the concentration of of the antigen and antibody-modified Nanozyme probes

This study determined the optimal detection sensitivity through a checkerboard titration of the antigen and the Au@Pt probe concentration. The data analysis presented in Table S2 revealed that the optimal OD value, which is generally accepted as suitable in the absence of AFB_1, was achieved when the antigen coating concentration was 0.25 μg/mL and the Au@Pt probe was diluted 15-fold, or when the antigen coating concentration was 0.125 μg/mL and the Au@Pt probe dilution factor was 10. Then, inhibition curves (Fig. S7) were generated using various concentrations of AFB_1 standard solution under the specified experimental parameters described above. Evaluation of the IC_{50} values from the two established inhibition curves revealed that the most favorable conditions for the immunoassay involved an antigen concentration of 0.25 μg/mL and a dilution factor of 15 for the Au@Pt probe.

3.8. Comparison of the sensitivity of PtNP-enhanced Au@Pt-ELISA with that of traditional ELISA

Owing to the commercialization of enzyme-labeled secondary antibodies, traditional indirect competitive ELISA (ic-ELISA) has become a commonly used method for high-throughput screening of mycotoxins. However, its practical applicability is somewhat limited because of its relatively low sensitivity and long detection time limit. Comparative analysis revealed that our newly established method has a detection

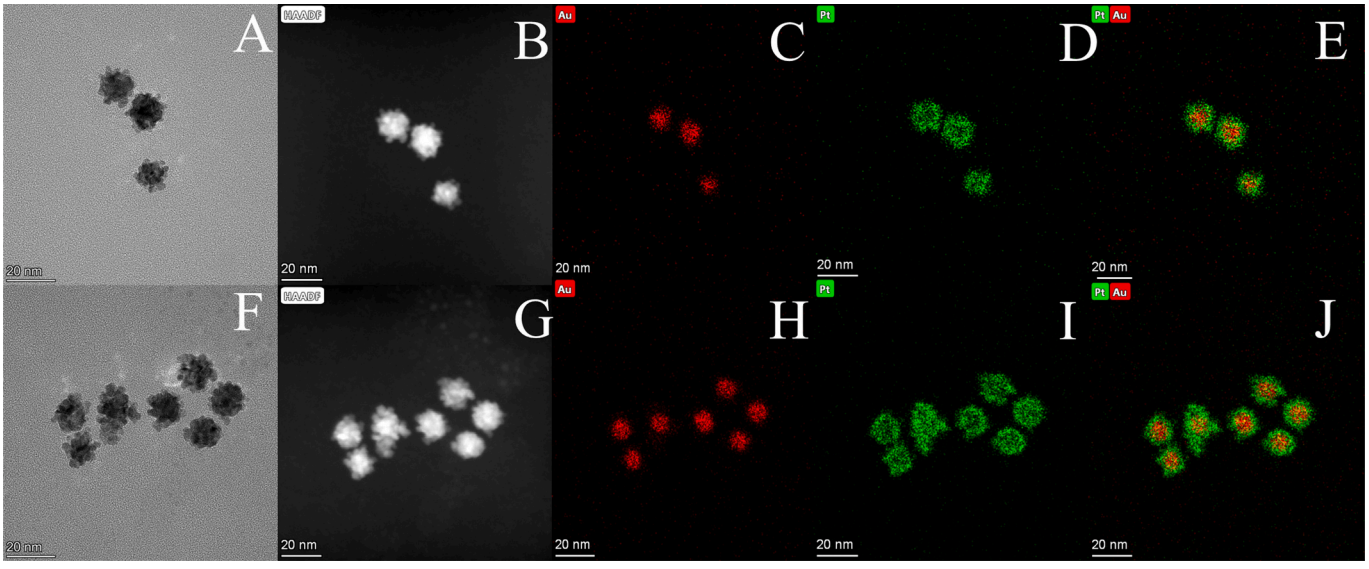

Fig. 3. HRTEM characterization of (A) Au@Pt probe and (F) PtNP-enhanced Au@Pt probe; HAADF-STEM and EDS mapping of Au@Pt probe (B-E) and PtNP-enhanced Au@Pt probe (G-J).

limit (LOD) that is approximately six times lower than that of conventional ic-ELISA (Fig. S8). Furthermore, our method adopts a direct competitive mode, eliminating the need for secondary antibodies, thereby reducing the detection time by approximately 1 h compared with that of ic-ELISA.

3.9. Sample analysis

3.9.1. Optimization of sample pretreatment methods for lotus seed powder

The primary chemical constituents in lotus seeds are flavonoids, organic acids, sterols, terpenoids, lipids, proteins, and carbohydrates (Arooj et al., 2021). These substances may be coextracted with AFB_1, consequently disturbing antigen–antibody recognition and causing inaccurate results, such as false-positives or false-negatives. Thus, developing an efficient sample pretreatment method to minimize matrix interference is vital for ensuring assay accuracy. In accordance with the findings of our prior investigation (Guan et al., 2022), we initially optimized the extraction solvent by evaluating the ratio of B_0 values between the matrix blank and the solvent blank and the ratio of inhibition rates between the matrix-spiked solution and the solvent-spiked solution with identical AFB_1 concentration. When the extraction solvent was 90 % acetonitrile, these two ratios were close to 1.0 (Table S3), indicating minimal matrix interference. Similarly, optimization of the dilution solvent revealed that the use of PBS containing 0.01 % Tween 20 resulted in the least matrix interference (Table S4). Therefore, we selected 90 % acetonitrile as the extraction solvent and PBS containing 0.01 % Tween 20 as the dilution solvent for subsequent experiments.

3.9.2. Method validation

To validate the accuracy of the PtNP-enhanced Au@Pt-ELISA, a lotus seed powder sample, which was previously confirmed to be negative by LC–MS/MS, was spiked with AFB_1 at various concentrations (2.5, 5, and 10 μg/kg). The recoveries of the fortified lotus seed powder samples were determined via PtNP-enhanced Au@Pt-ELISA, and the results are shown in Table S5. The recoveries ranged from 87.90 % to 92.45 %, with a relative standard deviation (RSD) of less than 14 %. These results meet the accuracy and precision requirements specified by COMMISSION REGULATION (EC) No 401/2006. On the basis of the definitions in the supplementary materials (Section S2), the LOD and limit of quantitation (LOQ) were determined to be 1.6 and 4.3 pg/mL, respectively, which are equivalent to 0.32 and 0.86 μg/kg in the initial solid samples. Notably, the LOD and LOQ of the nano-ELISA developed in this study satisfy the maximum limits (MLs) defined by COMMISSION REGULATION (EC) No 1881/2006. This regulation sets the limit for AFB_1 at 2 μg/kg in cereals and products derived from cereals. Moreover, they also meet the 5 μg/kg limit for lotus seeds specified in the Chinese Pharmacopoeia 2020 edition. The detection range was from 0.0043 to 0.131 ng/mL (with an inhibitory concentration range of 20–80 %), corresponding to 0.86–26.2 μg/kg in the initial solid samples.

Moreover, the specificity of the proposed immunoassay for AFB_1 detection was evaluated through the analysis of the cross-reactivity of three structural analogs of AFB_1 (AFB_2, AFG_1, and AFG_2), which are the analogs most likely to coexist with AFB_1. The cross-reaction rates of AFB_2, AFG_1, and AFG_2 were 39.93 %, 0.74 %, and 0.72 %, respectively (Fig. 4). These findings confirm the high specificity of the developed nanozyme-based ELISA method.

Finally, matrix effect assessment was conducted, which involved comparing the calibration curve slope derived from standard solutions with that derived from matrix-matched standard solutions. The slope ratio, which was obtained from the matrix-matched standard and the solvent standard curve, was found to be 0.97. This suggests that the sample's matrix effect was within acceptable levels. Thus, the matrix-matched curve could be replaced by a solvent curve in the analysis of real samples.

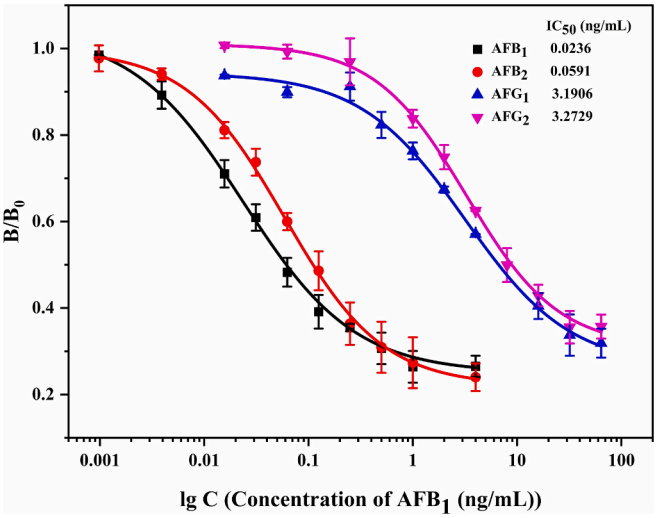

Fig. 4. Cross-reaction curves of AFB_1, AFB_2, AFG_1, and AFG_2.

3.10. Real samples detection

The established method was used to detect 18 batches of randomly purchased lotus seed powder samples. Among these samples, 13 batches were positive, with contamination levels between 3.23 and 249.95 μg/kg. The positive samples were also tested via the confirmatory LC–MS/MS method, and representative chromatograms are shown in Fig. S9. A correlation analysis was performed between the Au@Pt-ELISA results and the confirmatory LC–MS/MS data, which revealed a correlation coefficient of $r = 0.9888$, indicating the method's accuracy and reliability. This is depicted in Fig. S10. Lotus seed powder is obtained by grinding the seeds, which makes it difficult to judge its quality based on appearance. Our detection results revealed that the contamination rate of lotus seed powder is much higher than that of the raw lotus seed materials reported previously (Qin et al., 2020). Current research focuses predominantly on aflatoxin contamination in raw lotus seed materials, with limited data available regarding aflatoxins contamination in related lotus seed products, such as lotus seed powder. Given our findings, it is imperative to intensify research in this area to ensure food safety.

3.11. Comparison of the proposed Au@Pt-based ELISA with other reported immunoassays

In the development of nanomaterial-based immunoassays, the preparation of nanomaterial–antibody conjugate is a crucial step that significantly influences the performance of the detection method. To increase the reproducibility of the probe labeling process, this study employed a relatively simple electrostatic adsorption method, which, compared with covalent modification, presents distinct advantages in reducing the preparation time (as outlined in Table S6) and simplifying the operational steps. Furthermore, the data in Table S6 reveal that the detection sensitivity of the method developed in this research is higher than that of the previously reported AFB_1 rapid detection method for lotus seeds. Despite the detection time per assay being longer than those of some detection modes, such as immunochromatographic test strips, the advantage of this method is its ability to analyze nearly 25 samples simultaneously on a single microplate. This significantly increases the efficiency of high-throughput sample screening.

4. Conclusions

In summary, this research introduces a highly sensitive and convenient method for AFB_1 screening in lotus seed powder via PtNP-

enhanced Au@Pt-ELISA. The peroxidase-like activity of the Au@Pt probe, previously inhibited by attached antibodies, was significantly enhanced by the in situ deposition of PtNPs. This improvement allows for PtNP-enhanced Au@Pt as a signal amplification system instead of the conventional HRP system in ELISA, resulting in increased sensitivity. The LOD achieved was 1.6 pg/mL (0.32 μg/kg), approximately 6-fold lower than that of conventional ELISA. Furthermore, the direct competitive model of the proposed method simplified the operational steps, reducing the detection time by about an hour compared to traditional ic-ELISA. We also optimized the sample preparation procedure to minimize matrix interference and ensure assay accuracy. The obtained spiked recoveries ranged between 87.90 % and 92.45 %, with an RSD of less than 14 %, demonstrating good accuracy and precision. Lastly, a quantitative analysis of AFB_1 in 18 batches of lotus seed powder samples was conducted, and the results were strongly correlated with the LC–MS/MS results. While numerous analytical techniques have been devised for the rapid detection of small-molecule compounds via the catalytic activity of nanozymes, to the best of our knowledge, this study represents the first report of increasing the catalytic efficacy of nanozymes by employing in situ deposition of PtNPs. This straightforward and efficient signal amplification approach may serve as a reference for developing other analytical methods utilizing nanozymes as recognition elements and signal markers.

CRediT authorship contribution statement

Lei Zhang: Writing – review & editing, Writing – original draft, Funding acquisition, Conceptualization. **Huiqiang Huang:** Writing – original draft, Validation, Methodology. **Mengyao Liao:** Writing – original draft, Methodology. **Chenghua Luo:** Methodology. **Qiuyue Wu:** Formal analysis. **Rentang Huang:** Formal analysis. **Hongmei Liu:** Validation. **Xiangsheng Zhao:** Writing – review & editing, Funding acquisition, Conceptualization. **Shumei Wang:** Writing – review & editing, Supervision, Conceptualization.

Declaration of competing interest

The authors declare that they have no known competing financial interests or personal relationships that could have appeared to influence the work reported in this paper.

Data availability

No data was used for the research described in the article.

Acknowledgements

This research was funded by the National Natural Science Foundation of China (82374032, 82074130), the Guangdong Basic and Applied Basic Research Foundation (2022A1515012099), and the Innovation Project of the Guangdong Provincial Department of Education (2023KTSCX059).

Appendix A. Supplementary data

Supplementary data to this article can be found online at https://doi.org/10.1016/j.fochx.2024.102030.

References

Arooj, M., Imran, S., Inam-ur-Raheem, M., Rajoka, M. S. R., Sameen, A., Siddique, R., … Aadil, R. M. (2021). Lotus seeds (Nelumbinis semen) as an emerging therapeutic seed: A comprehensive review. *Food Science & Nutrition, 9*(7), 3971–3987. https://doi.org/10.1002/fsn3.2313

Cao, J., Yu, X., Deng, Z., Pan, Y., Zhang, B., Tsao, R., & Li, H. (2018). Chemical compositions, Antiobesity, and antioxidant effects of Proanthocyanidins from Lotus seed Epicarp and Lotus seed pot. *Journal of Agricultural and Food Chemistry, 66*(51), 13492–13502. https://doi.org/10.1021/acs.jafc.8b05137

Chu, X., Dou, X., Kong, W., Yang, M., Zhao, C., Zhao, M., & Ouyang, Z. (2015). Contamination level of aflatoxin B1 in lotus seeds rapid screening by indirect competitive ELISA method. *China Journal of Chinese Materia Medica, 40*(4), 704–709. https://doi.org/10.4268/cjcmm20150424

Deng, H.-H., Weng, S.-H., Huang, S.-L., Zhang, L.-N., Liu, A.-L., Lin, X.-H., & Chen, W. (2014). Colorimetric detection of sulfide based on target-induced shielding against the peroxidase-like activity of gold nanoparticles. *Analytica Chimica Acta, 852*, 218–222. https://doi.org/10.1016/j.aca.2014.09.023

Deng, K., Zhang, Y., Xiao, H., Hou, Y., Xu, Q., Li, Y., … Ma, L. (2024). Nafion-immobilized functionalized MWCNT-based electrochemical Immunosensor for aflatoxin B1 detection. *ACS Omega, 9*(8), 8754–8762. https://doi.org/10.1021/acsomega.3c04619

Dunno, K., Kumar, M., Mostafa, H., Maqsood, S., & Bangar, S. P. (2022). A comprehensive review on lotus seeds (*Nelumbo nucifera* Gaertn.): Nutritional composition, health-related bioactive properties, and industrial applications. *Journal of Functional Foods, 89*, 16. https://doi.org/10.1016/j.jff.2022.104937

Elamin, A., Sultana, S., & Sakuda, S. (2024). Evaluation of the susceptibility of Lotus seeds (*Nelumbo nucifera* Gaertn.) to aspergillus flavus infection and aflatoxin contamination. *Toxins, 16*(1), 29. https://doi.org/10.3390/toxins16010029

Feng, J., Huang, P., & Wu, F.-Y. (2017). Gold–platinum bimetallic nanoclusters with enhanced peroxidase-like activity and their integrated agarose hydrogel-based sensing platform for the colorimetric analysis of glucose levels in serum. *Analyst, 142*(21), 4106–4115. https://doi.org/10.1039/C7AN01343D

Gao, Z., Xu, M., Hou, L., Chen, G., & Tang, D. (2013). Irregular-shaped platinum nanoparticles as peroxidase mimics for highly efficient colorimetric immunoassay. *Analytica Chimica Acta, 776*, 79–86. https://doi.org/10.1016/j.aca.2013.03.034

Guan, K., Huang, R., Liu, H., Huang, Y., Chen, A., Zhao, X., … Zhang, L. (2022). Development of a reliable ic-ELISA with a robust Antimatrix interference capability based on QuEChERS Technology for the Rapid Detection of Zearalenone in edible and medical Coix seeds and subsequent risk assessments. *Foods, 11*(19), 2983. https://doi.org/10.3390/foods11192983

He, W., Liu, Y., Yuan, J., Yin, J.-J., Wu, X., Hu, X., … Guo, Y. (2011). Au@Pt nanostructures as oxidase and peroxidase mimetics for use in immunoassays. *Biomaterials, 32*(4), 1139–1147. https://doi.org/10.1016/j.biomaterials.2010.09.040

Hendrickson, O. D., Zvereva, E. A., Pridvorova, S. M., Dzantiev, B. B., & Zherdev, A. V. (2023). The use of Au@Pt nanozyme to perform ultrasensitive immunochromatographic detection of banned pork additives in meat products. *Food Control, 154*, Article 110013. https://doi.org/10.1016/j.foodcont.2023.110013

Huang, R., Huang, Y., Liu, H., Guan, K., Chen, A., Zhao, X., … Zhang, L. (2023). A bifunctional AuNP probe-based enzyme-linked immunosorbent assay for facile and ultrasensitive detection of trace zearalenone in coix seed. *Microchemical Journal, 184*, Article 108152. https://doi.org/10.1016/j.microc.2022.108152

Jia, B., Liao, X., Sun, C., Fang, L., Zhou, L., & Kong, W. (2021). Development of a quantum dot nanobead-based fluorescent strip immunosensor for on-site detection of aflatoxin B1 in lotus seeds. *Food Chemistry, 356*, 129614. https://doi.org/10.1016/j.foodchem.2021.129614

Jv, Y., Li, B., & Cao, R. (2010). Positively-charged gold nanoparticles as peroxidiase mimic and their application in hydrogen peroxide and glucose detection. *Chemical Communications, 46*(42), 8017–8019. https://doi.org/10.1039/C0CC02698K

Lee, Y., Loew, A., & Sun, S. (2010). Surface- and structure-dependent catalytic activity of Au nanoparticles for oxygen reduction reaction. *Chemistry of Materials, 22*(3), 755–761. https://doi.org/10.1021/cm9013046

Li, H., Wu, Y., Xu, Z., & Wang, Y. (2024). Controllable preparation of a Cu NCs@Zn-MOF hybrid with dual emission induced by an ion exchange strategy for the detection of explosives. *ACS Sensors, 9*(9), 4701–4710. https://doi.org/10.1021/acssensors.4c01093

Li, J., Liu, F., Zhu, Z., Liu, D., Chen, X., Song, Y., … Yang, C. (2018). In situ Pt staining method for simple, stable, and sensitive pressure-based bioassays. *ACS Applied Materials & Interfaces, 10*(16), 13390–13396. https://doi.org/10.1021/acsami.8b03567

Li, W., Chen, B., Zhang, H., Sun, Y., Wang, J., Zhang, J., & Fu, Y. (2015). BSA-stabilized Pt nanozyme for peroxidase mimetics and its application on colorimetric detection of mercury(II) ions. *Biosensors and Bioelectronics, 66*, 251–258. https://doi.org/10.1016/j.bios.2014.11.032

Liu, S., Qiu, F., Kong, W., Wei, J., Xiao, X., & Yang, M. (2013). Development and validation of an accurate and rapid LC-ESI-MS/MS method for the simultaneous quantification of aflatoxin B1, B2, G1 and G2 in lotus seeds. *Food Control, 29*(1), 156–161. https://doi.org/10.1016/j.foodcont.2012.05.069

Lou, D., Tian, Y., Zhang, Y., Yin, J., Yang, T., He, C., … Gu, N. (2018). Peroxidase-like activity of gold nanoparticles and their gold staining enhanced ELISA application. *Journal of Nanoscience and Nanotechnology, 18*(2), 951–958. https://doi.org/10.1166/jnn.2018.13977

Magdalena Pisoschi, A. I., Florin, Stanca, L., Ionescu Petcu, A., Purdoiu, L., Ionut Geicu, O., … Iren Serban, A. (2023). Comprehensive overview and critical perspective on the analytical techniques applied to aflatoxin determination – A review paper. *Microchemical Journal, 191*, Article 108770. https://doi.org/10.1016/j.microc.2023.108770

Mora-Sanz, V., Saa, L., Briz, N., & Pavlov, V. (2020). Synthesis and characterization of antibody-protected bimetallic nanoclusters with catalytic properties. *Chemistry of Materials, 32*(19), 8286–8293. https://doi.org/10.1021/acs.chemmater.0c02096

Park, K. S., Kim, M. I., Cho, D.-Y., & Park, H. G. (2011). Label-free colorimetric detection of nucleic acids based on target-induced shielding against the peroxidase-mimicking

activity of magnetic nanoparticles. *Small, 7*(11), 1521–1525. https://doi.org/10.1002/smll.201001886

Qin, L., Jiang, J.-Y., Zhang, L., Dou, X.-W., Ouyang, Z., Wan, L., & Yang, M.-H. (2020). Occurrence and analysis of mycotoxins in domestic Chinese herbal medicines. *Mycology, 11*(2), 126–146. https://doi.org/10.1080/21501203.2020.1727578

Saud Al-Bagmi, M., Shahnawaz Khan, M., Alhasan Ismael, M., Al-Senaidy, A. M., Ben Bacha, A., Mabood Husain, F., & Alamery, S. F. (2019). An efficient methodology for the purification of date palm peroxidase: Stability comparison with horseradish peroxidase (HRP). *Saudi Journal of Biological Sciences, 26*(2), 301–307. https://doi.org/10.1016/j.sjbs.2018.04.002

Taron, W., Jamnongkan, W., Techasen, A., Phetcharaburanin, J., Namwat, N., Sithithaworn, P., … Ngeontae, W. (2020). AuNPs-LISA, an efficient detection assay for *Opisthorchis viverrini* (Ov) antigen in urine. *Talanta, 209*, Article 120592. https://doi.org/10.1016/j.talanta.2019.120592

Villalba-Rodríguez, A. M., Martínez-Zamudio, L. Y., Martínez, S. A. H., Rodríguez-Hernández, J. A., Melchor-Martínez, E. M., Flores-Contreras, E. A., … Parra-Saldívar, R. (2023). Nanomaterial constructs for catalytic applications in biomedicine: Nanobiocatalysts and Nanozymes. *Topics in Catalysis, 66*(9–12), 707–722. https://doi.org/10.1007/s11244-022-01766-4

Wang, W., Zou, Y., Yan, J., Liu, J., Chen, H., Li, S., & Zhang, L. (2018). Ultrasensitive colorimetric immunoassay for hCG detection based on dual catalysis of Au@Pt core–shell nanoparticle functionalized by horseradish peroxidase. *Spectrochimica Acta Part A: Molecular and Biomolecular Spectroscopy, 193*, 102–108. https://doi.org/10.1016/j.saa.2017.12.014

Wei, D., Zhang, X., Chen, B., & Zeng, K. (2020). Using bimetallic Au@Pt nanozymes as a visual tag and as an enzyme mimic in enhanced sensitive lateral-flow immunoassays: Application for the detection of streptomycin. *Analytica Chimica Acta, 1126*, 106–113. https://doi.org/10.1016/j.aca.2020.06.009

Xiong, J., Wen, D., Zhou, H., Chen, R., Wang, H., Wang, C., … Wu, L. (2022). Occurrence of aflatoxin M1 in yogurt and milk in Central-Eastern China and the risk of exposure in milk consumers. *Food Control, 137*, Article 108928. https://doi.org/10.1016/j.foodcont.2022.108928

Yu, Y. P., Lai, S. J., Chang, C. R., Chen, W. C., Wu, S. H., & Lu, C. P. (2021). Peptidomic analysis of low molecular weight antioxidative peptides prepared by lotus (*Nelumbo nucifera* Gaertn.) seed protein hydrolysates. *LWT- Food Science and Technology, 144*, 7. https://doi.org/10.1016/j.lwt.2021.111138

Yuan, J., Takae, K., & Tanaka, H. (2022). Impact of charge regulation on self-assembly of Zwitterionic nanoparticles. *Physical Review Letters, 128*(15), Article 158001. https://doi.org/10.1103/PhysRevLett.128.158001

Zeng, H., He, S., Xiong, Z., Su, J., Wang, Y., Zheng, B., & Zhang, Y. (2023). Gut microbiota-metabolic axis insight into the hyperlipidemic effect of lotus seed resistant starch in hyperlipidemic mice. *Carbohydrate Polymers, 314*, Article 120939. https://doi.org/10.1016/j.carbpol.2023.120939

Zeng, R., Luo, Z., Su, L., Zhang, L., Tang, D., Niessner, R., & Knopp, D. (2019). Palindromic molecular Beacon based Z-scheme BiOCl-Au-CdS Photoelectrochemical biodetection. *Analytical Chemistry, 91*(3), 2447–2454. https://doi.org/10.1021/acs.analchem.8b05265

Zhang, C., Hu, J., Wu, X., Shi, J., & Hammock, B. D. (2022). Development of the Au@Pt-labeled Nanobody lateral-flow Nanozyme immunoassay for visual detection of 3-Phenoxybenzoic acid in Milk and Lake water. *ACS Agricultural Science & Technology, 2*(3), 573–579. https://doi.org/10.1021/acsagscitech.2c00018

Zhang, J., & Liu, J. (2020). Nanozyme-based luminescence detection. *Luminescence, 35*(8), 1185–1194. https://doi.org/10.1002/bio.3893

Zhang, T., Tian, F., Long, L., Liu, J., & Wu, X. (2018). Diagnosis of rubella virus using antigen-conjugated Au@Pt nanorods as nanozyme probe. *International Journal of Nanomedicine, 13*, 4795–4805. https://doi.org/10.2147/ijn.S171429

Zheng, J.-N., Li, S.-S., Ma, X., Chen, F.-Y., Wang, A.-J., Chen, J.-R., & Feng, J.-J. (2014). Popcorn-like PtAu nanoparticles supported on reduced graphene oxide: Facile synthesis and catalytic applications. *Journal of Materials Chemistry A, 2*(22), 8386–8395. https://doi.org/10.1039/C4TA00857J

Zhu, Z., Guan, Z., Liu, D., Jia, S., Li, J., Lei, Z., … Yang, C. J. (2015). Translating molecular recognition into a pressure signal to enable rapid, sensitive, and portable biomedical analysis. *Angewandte Chemie International Edition, 54*(36), 10448–10453. https://doi.org/10.1002/anie.201503963